Chromone scaffold–mediated reprogramming of the epithelial–mesenchymal transition prevents fibrosis

Han-Soo Kim,[1,2*] Jun-Hwan Kim,[3*] Young-Min Yoon,[3] Moon Kee Meang,[4] Ji Yong Lee,[5] Tae Hee Lee,[6] Ik-Hwan Kim,[4] and Byung-Soo Youn[3#]

[1]Department of Biomedical Sciences, Catholic Kwandong University College of Medicine, Gangneung-si, Gangwon-do 25601, Republic of Korea; [2]Institute for Healthcare and Life Science, International St. Mary's Hospital and College of Medicine, Catholic Kwandong University, Incheon 22711, Republic of Korea; [3]OsteoNeuroGenInc, Seoul, 08501, Republic of Korea; [4]Department of Biotechnology, Korea University, Seoul 02841, Republic of Korea; [5]Department of Anatomy, Yonsei University Wonju College of Medicine, Wonju-si, Gangwon-do 26426, Republic of Korea; [6]Formulae Pharmacology Department, School of Oriental Medicine, Gachon University, Seongnam-si, Gyeonggi-do, Republic of Korea 13120

Running title: *Reversion of fibrosis by eupatilin*

[*]These authors contributed equally to this work.

[#]To whom correspondence should be addressed: OsteoNeuroGen Inc. Ace High-end Tower 9th 233, Gasandigital-1-ro, Geumcheon-gu, Seoul, 08501, Republic of Korea; byung4jc@gmail.com; Tel. +82-2-6267 2737; Fax. +82-2-6267-2740

Key words: chromone scaffold, epithelial–mesenchymal transition, eupatilin, lung fibrosis, myofibroblasts

---

Abstract

Fibrotic diseases are major causes of morbidity and mortality, and the epithelial–mesenchymal transition (EMT) plays a central role in the development of tissue/organ fibrosis. We discovered that eupatilin, a member of the chromone scaffold (CS)-containing family of compounds found ubiquitously in the plant kingdom, completely reversed fibrogenesis *in vitro* and substantially ameliorated bleomycin-induced lung fibrosis (BILF). Furthermore, eupatilin induced growth arrest and morphological changes in primary fibroblasts derived from a patient with idiopathic pulmonary fibrosis (IPF). To better understand fibrosis, we established a mouse hepatic stellate cell (HSC) line that robustly differentiated into myofibroblasts upon treatment with TGFβ. HSC fibrogenesis was completely blocked by eupatilin, which caused dramatic morphological changes while inhibiting expression of EMT-related genes. The chemical groups linked to C2, C3, C6, and C7 on the CS of eupatilin were essential for its anti-fibrogenic effects. Unlike eupatilin, pirfenidone failed to block HSC fibrogenesis and did not affect the morphology of HSCs or lung fibroblasts. Although pirfenidone affected local production of TGFβ, as reflected by a reduction in the TGFβ level in lung lysates of BILF model mice, eupatilin is likely to act via a different therapeutic mechanism. In particular, eupatilin had greater anti-fibrotic capacity and EMT-inhibitory activity, and significantly attenuated the phosphorylation of Erk. Based on the interactome we constructed, *Integrinβ3* is a major player in integration of TGFβ signaling and eupatilin-mediated anti-fibrosis. Our findings suggest that combinatorial use of eupatilin and pirfenidone may augment the therapeutic efficacy of IPF treatment.

Fibrosis is a complex disease state in which elevated proliferation of myofibroblasts is accompanied by overproduction of extracellular matrix (ECM) components (1). Two fibrotic conditions, idiopathic pulmonary fibrosis (IPF) and liver fibrosis preceded by non-alcoholic steatohepatitis (NASH), affect many people around the world, and thus represent an urgent medical need. To date, however, no curative drugs for these conditions have become available

(2,3). Two small-molecule anti-fibrotic drugs, pirfenidone (Esbriet) and nintedanib (Ofev), have recently been approved for IPF (4), but their efficacies and side effects must be improved to successfully treat this disease. Moreover, the underlying molecular and cellular mechanisms through which these drugs exert their anti-fibrotic activities remain to be elucidated.

Flavones are members of the polyphenol family, a group of >10,000 compounds predominantly found in the plant kingdom (5). In general, these phytochemicals protect plants from radiation damage (6). Due to their anti-oxidant and anti-inflammatory potentials, flavones have long been used to treat inflammatory diseases such as arthritis and asthma (7). Chromone, 1,4-benzopyrone-4-one, is a chemical scaffold present in flavones (8), and the chromone derivatives (CDs) are a diverse family based on this core chemical framework (9). We recently reported that eupatilin, a CD from an *Artemisia* species, dramatically inhibits osteoclastogenesis (10) and downregulates multiple genes associated with the epithelial–mesenchymal transition (EMT). Specifically, 24 of the 50 top genes differentially regulated by eupatilin are associated with the EMT, prompting us to hypothesize that eupatilin can prevent fibrosis (Figure S1).

Here, we show that eupatilin can block induction of EMT and alter cell shape, thereby substantially ameliorating lung fibrosis. This observation opens the door to a powerful new therapeutic modality for treating IPF.

Results and discussion

Eupatilin has potent anti-fibrogenic capacity

We first investigated whether TGFβ-mediated fibrogenesis could be inhibited by CDs, particularly eupatilin, in human lung fibroblasts derived from IPF patients (hereinafter DHLFs: Diseased Human Lung Fibroblasts) (11). Compared with TGFβ alone, co-stimulation of DHLFs with TGFβ plus eupatilin resulted in significant growth arrest and morphological change (Figure 1A and S2A). Currently, pirfenidone and nintedanib are the only targeted drugs approved for use in treating IPF (12). Two different concentrations of nintedanib completely blocked myofibroblastogenesis, whereas pirfenidone had no effect (Figure S2B).

To examine the influence of these compounds on the EMT, we performed immunocytochemistry (ICC) to detect expression of α-smooth muscle actin (αSMA), a marker of EMT induction. DHLFs, presumably preconditioned in IPF patients, had a myofibroblast-like morphology *in vitro*, and could be inferred to intrinsically express αSMA, which was slightly upregulated by TGFβ (Figure 1B). Co-stimulation of DHLFs with eupatilin and TGFβ, however, eliminated αSMA expression (Figure 1B). Among the EMT-associated genes upregulated in DHLFs are those encoding vimentin and periostin; the latter is an important regulator of ECM biogenesis that also serves as a ligand for integrin αVβ3 (13). TGFβ substantially increased expression of both genes, but eupatilin negated their upregulation (Figure 1C).

A549 cells are a human lung adenocarcinoma cell line of alveolar basal epithelial cell origin that have been used for analysis of tumor metastasis and the EMT (14). TGFβ rendered A549 cells somewhat blastogenic and caused them to significantly upregulate *Snail* and *Vimentin*, but these effects were substantially attenuated by eupatilin (Figure S3). Moreover, cell morphology changed dramatically, with the cells becoming rounder, suggesting that eupatilin can reorganize cytoskeletal structures. Taken together, these data suggest that eupatilin inhibits proliferation and drives morphological change of DHLFs, thereby negatively regulating EMT. In previous work, we demonstrated that eupatilin does not promote cell death (10).

Myofibroblasts play a pivotal role in collagen deposition in fibrotic tissues. Differentiation of several progenitor cell types has been observed in lung tissues, but reports of *in vitro* lung fibrogenesis remain limited (15). To develop an efficient cell-based fibrogenesis assay, we established a mouse hepatic stellate cell (HSC) line, ONGHEPA1 (Figure S4). HSCs are widely appreciated for their unique roles in initiation and perpetuation of liver fibrosis (16). ONGHEPA1 had a mesenchymal morphology, expressed GATA4 but not cytokeratin 18 (Figure S4A and S4B), and expressed CD29, CD44, and CD106 on the cell surface (Figure S4C), strongly

indicating that they are of mesenchymal origin. Based on these features, we concluded that ONGHEPA1 is a mouse primary HSC line.

When ONGHEPA1 cells were stimulated with TGFβ, full differentiation into myofibroblasts occurred within 12–24 hr, but eupatilin completely inhibited TGFβ-induced fibrogenesis at concentrations of 50 μM or higher (Figure S5A). However, pretreatment of ONGHEPA1 with eupatilin for 1–6 hr did not diminish fibrogenesis, suggesting that TGFβ-elicited signal transduction in combination with eupatilin is necessary to blunt fibrogenesis (Figure S5B). Eupatilin did not alter phosphorylation of Smad2 or Akt, but it significantly inhibited phosphorylation of Erk and marginally inhibited Smad3 after 12 hr of treatment; Erk phosphorylation recovered slightly at 24 hr (Figure S6), an observation we do not currently understand. Erk (17) and Smad3 (18) play pivotal roles in TGFβ-mediated induction of the EMT.

PDGFR signaling has also been implicated in fibrogenesis (19). However, when ONGHEPA1 cells were subjected to differentiation, PDGF was incapable of driving differentiation in the presence of eupatilin (Figure S7A and S7B). ICC experiments clearly demonstrated that strong αSMA immunoreactivity induced by TGFβ stimulation was eliminated by eupatilin (Figure 1D), and the same pattern held true for real-time expression of *Col11α1* (Figure 1D).

Nintedanib is an angiokinase inhibitor that antagonizes TGFβR, FGFR, and PDGFR, but the mode of action (MOA) of pirfenidone remains elusive (20). When we stimulated cells with TGFβ in the presence of one of these drugs, or eupatilin, we observed that eupatilin and nintedanib effectively curbed fibrogenesis by ONGHEPA1 cells, as in the case of DHLFs, albeit with slight morphological differences between the two drugs (Figure 1E). On the other hand, pirfenidone could not inhibit differentiation, implying that the MOAs of eupatilin and pirfenidone differ in this *in vitro* differentiation setup. The degree of inhibition of αSMA mirrored the anti-fibrogenic effects (Figure 1F). Taken together, these observations demonstrate that the chromone scaffold (CS) compound eupatilin is a potent anti-fibrotic drug that can inhibit fibrogenesis during differentiation of HSCs into myofibroblasts and reprogram the EMT, leading to cell shape change. This conclusion, in conjunction with the eupatilin-associated growth arrest and morphological changes in DHLFs, prompted us to investigate whether eupatilin could exert a therapeutic effect on IPF. For this purpose, we used the mouse bleomycin-induced lung fibrosis (BILF) model.

Eupatilin significantly improved BILF

Eupatilin or pirfenidone at 100 mg/kg (mpk) was orally administered twice per day, followed by one intratracheal administration of bleomycin; daily oral drug intake continued for the next 14 days (Figure S8). Each drug administration group consisted of eight mice. We observed significant reductions in the levels of soluble collagen and hydroxyproline, as well as changes in histomorphometry, in the drug-treated animals (Figure S8A, S8B, and S8C). Interestingly, the largest reduction in TGFβ production occurred in the pirfenidone-treated mice (Figure S8D), suggesting that the MOA of pirfenidone involves downregulation of TGFβ production, presumably from immune cells. Fibrotic tissues are characterized by notable collagen deposition, along with proliferation or infiltration of myofibroblasts (21). To examine these processes, we performed H&E staining in such a way as to visibly stain proliferative and infiltrated cells, and used Sirius red to stain regions of collagen deposition. As seen in Figure S8E, bleomycin-treated lungs harbored the largest number of H&E- and Sirius red–stained cells, and pirfenidone treatment weakened the intensities of both stains. More intriguingly, eupatilin-treated lungs contained the smallest number of fibrotic cells and very pale collagen staining, suggesting that the drug has a potent anti-fibrotic effect (Figure S8E).

Next, to confirm the anti-fibrotic potential of eupatilin, we examined the dose dependence of its effects. At doses of 100 and 200 mpk, but not a lower dose of 50 mpk, we observed a statistically significant improvement in the levels of soluble collagen and hydroxyproline. Overall, 100 mpk pirfenidone had less of an inhibitory effect on collagen morphometry, soluble collagen, and

hydroxyproline than 200 mpk eupatilin, and this difference was also statistically significant (Figure 2A and 2B). Notably in this regard, the molar concentration of 200 mpk eupatilin is similar to that of 100 mpk pirfenidone, suggesting that eupatilin is a more potent anti-fibrotic agent. As before, 100 mpk pirfenidone was associated with a smaller amount of TGFβ production in comparison with eupatilin (Figure 2C), again suggesting that the MOA of pirfenidone involves decreasing the production of TGFβ in the lung. Eupatilin seems to be efficiently absorbed into the upper GI tract and appears in plasma within 1 hr of ingestion, and is also readily detected in lung tissue lysates (22). We found that glucuronide-eupatilin was the major metabolite in plasma, whereas free eupatilin predominated in lung tissues. This observation suggests that orally administered eupatilin is rapidly disseminated to the lung via glucuronidation followed by deconjugation of the glucuronide moiety (Figure S9A). However, lung pharmacokinetics (PK) analysis readily detected free eupatilin, as seen in Figure S9B. Eupatilin existed in the lung exclusively as the free form, but at concentrations at least 50-fold lower than those of pirfenidone, suggesting that eupatilin is an extremely potent drug against lung fibrosis. Lung tissues express high levels of deconjugating enzymes (23). Pirfenidone is hepatotoxic at high concentrations (24), whereas the toxicity of eupatilin remains unknown. To explore this issue, we performed a full set of liver function tests using mouse plasma. As shown in Figure S10, we detected no hepatotoxicity from mice treated with either 100 mpk pirfenidone or 200 mpk eupatilin, suggesting that eupatilin is a safe anti-fibrotic drug.

To determine whether eupatilin has anti-fibrotic efficacy, we performed a therapeutic efficacy test on BILF model mice, as schematized in Figure S11A. Soluble collagen production, collagen histomorphometry, and TGFβ production were measured in the lung lysates. We observed significant reductions in collagen levels at higher doses of eupatilin (100 and 200 mpk), but not at a lower dose (50 mpk); 100 mpk pirfenidone also had significant anti-fibrotic activity (Figure S11B and S11C). Consistent with the therapeutic efficacy of 100 mpk eupatilin, inhibition of TGFβ production by pirfenidone was somewhat lower than that induced by 200 mpk eupatilin (Figure S11D). This observation indicates that the MOA of eupatilin and pirfenidone may differ *in vivo*, consistent with the results of the *in vitro* fibrogenesis assay in ONGHEPA1 cells. Based on these observations, eupatilin has a comparable or higher anti-fibrotic capacity than pirfenidone, and the two drugs may have distinct MOAs.

Specific carbons of the CS and chemical residues are critical for anti-fibrogenic effects

The CS of eupatilin, shown by the highlighted carbons in Figure 3A, is linked to a phenyl ring coupled to two methoxy residues. The critical carbon residues for anti-fibrogenic potential are represented in colored fonts: C2 (green), C3 (purple), and C6 (red). Next, we selected 34 CDs based on chemical similarities to eupatilin, classified into five chemical groups (A through E), and evaluated their anti-fibrogenic effects (Figure 3E). Among them, three CDs had anti-fibrogenic activity: eupatilin; ONGE200, also known as hispidulin; and ONGA200, also known as jaceosidin. The latter two compounds are the most closely chemically related to eupatilin among the CDs tested. All of these compounds belong to group A, whose members differ in terms of the chemical residues coupled to the phenyl ring. Eupatilin and ONGE200 had marked anti-fibrotic effects (Figure S12A), whereas ONGA300 was cytotoxic at 50 μM (Figure S12B). ONGI300, in which two hydroxy groups are coupled to the phenyl ring, had weak anti-fibrogenesis activity and promoted cell death, suggesting that chemical alteration of the phenyl ring affects anti-fibrotic activity (Figure S12C).

To explore the importance of the eight carbons of the CS in terms of structure–function relationship, three anti-fibrotic CDs (eupatilin, ONGE200 and ONGA300) were brought into focus along with the remaining CDs. When a methoxy residue was coupled to C3, as in ONGH300, the anti-fibrotic effect was eliminated and toxicity was apparent (Figure 3C). In comparison with ONGE200, ONGI200 (also known as apigenin) lacks only the methoxy group coupled to C6. ONGI200 had no anti-fibrotic effect, suggesting that C6 is an important

constituent of the CS and that methoxylation of this position is necessary to prevent fibrosis (Figure 3D). We also noticed that ONGC200, in which the hydroxy residue of ONGE200 is replaced with a methoxy group, completely lost the anti-fibrotic effect, suggesting the C7 is also a critical component of the CS (Figure S13A). In addition, methoxylation at C2 of ONGA300, yielding a compound equivalent to ONGH300, abolished anti-fibrotic capacity, suggesting that the presence of a bulky group at C2 may affect anti-fibrogenic potential (Figure S13B). The same held true for ONGD400, a highly cytotoxic stereoisomer of ONGH300 (Figure S12C). The chemical residues affecting anti-fibrotic potential are detailed in Figure 3E. Taken together, our data confirm that chemical modifications on the CS are only tolerated at specific carbons, indicating a stringent structure–activity relationship in regard to the anti-fibrogenic effects of these compounds.

Reprogramming of the EMT by eupatilin may be responsible for anti-fibrosis

We next asked whether eupatilin blocks EMT induced by TGFβ. To this end, we stimulated ONGHEPA1 cells with TGFβ or TGFβ plus eupatilin, and then conducted global gene expression analyses by RNA-seq. Using a bioinformatics approach, we constructed an unbiased interactome that contained several notable hubs, including the collagen gene family (*Col11α1*) and the genes encoding components of the cytoskeleton (*Actin α smooth muscle aorta*, *Troponin 1* and *2*, *Tropomyosin 2*, *Myosin-heavy chain 1* and *Myosin-light chain 9*, and *Laminin 4*) (Figure S14). Notably, *integrin α1* and *integrin β3* played pivotal roles in connecting these hubs. Expression of *Slug*, a major transcription factor deeply involved in the EMT, was inhibited by eupatilin. Several genes encoding receptors, including members of the semaphorin receptor family, a cholesterol receptor (*Vldr*), and *CD44*, formed significant hubs. One notable signaling molecule associated with eupatilin-mediated reprogramming of the EMT was adenylate cyclase 9 (*Adcy9*), which is involved in small G-protein activation.

These observations indicate that eupatilin curbs induction of fibrosis by TGFβ, primarily by reprogramming the EMT, altering cell shape, and (to a lesser extent than pirfenidone) inhibiting TGFβ production. Therefore, eupatilin could be used for monotherapy or in combinatorial therapy with pirfenidone, with the goal of achieving synergistic therapeutic efficacy against IPF.

Experimental procedures

RNA-seq processing, differential gene expression analysis, and interactome analysis

Processed reads were mapped to the *Mus musculus* reference genome (Ensembl 77) using Tophat and Cufflink with default parameters (25). Differential analysis was performed using Cuffdiff (25) using default parameters. Further, FPKM values from Cuffdiff were normalized and quantitated using the R Package Tag Count Comparison (TCC) (26) to determine statistical significance (e.g., P values) and differential expression (e.g., fold changes). Gene expression values were plotted in various ways (i.e., Scatter, MA, and Volcano plots), using fold-change values, using an R script developed in-house. The protein interaction transfer procedure was performed using the STRING database (27) with the differentially expressed genes. A 60 Gb sequence was generated, and 10,020 transcripts were read and compared.

Effects of drugs on bleomycin-induced lung tissue fibrosis

All animal experiments were approved and performed in compliance with the IACUC at Woojung BSC (Suwon, Korea, Association for Assessment and Accreditation of Laboratory Animal Care-Accredited facility) under IRB-13023. C57BL/6J mice were anesthetized by inhalation of 70% N_2O and 30% O_2 gas containing 1.5% isoflurane. Fifty microliters of bleomycin solution in distilled water was directly injected into the lungs, all at once, via the aperture. Immediately after injection, the mice were allowed to recover from the anesthetic, and then housed in normal cages. Bleomycin (0.03U BLM in 50μl saline) was administered once using a visual instillobot. Twelve days after the administration of bleomycin, eupatilin was forcibly nasally administered via a micropipette, once a day (five times a week) for 1 week. Eupatilin was

dissolved in DPBS buffer (containing 1% DMSO), and 1 ml/kg was administered based on the most recent body weight. For 2 to 3 days after administration of eupatilin, mice were monitored for toxic symptoms or death, but no abnormal symptoms were observed. Three mice per test group were selected, and their lung tissues were excised. The lung tissues were stained with Masson's trichrome and observed under a microscope. Results were expressed as mean values and standard deviations. One hour before sacrifice, a final dose of eupatilin or pirfenidone was administered for plasma or lung PK. The bleomycin-treated mice exhibited a rapid decline in weight, but the sham control behaved normally. Eupatilin- or pirfenidone-administered mice exhibited weight gain from day 3 onward. Control and eupatilin-treated mice data were compared using Student's *t*-test. "Differences between samples were considered statistically significant when $p<0.05$.

Acknowledgments

The authors would like to thank Prof. Ho-Sup Yoon (Nanyang Technological University, Singapore) for insightful comments on the paper. This study was supported by an intramural fund from OsteoNeuroGen Inc.

Competing financial interests

H-S Kim, I-K Kim, and B-S Youn retain shares of OsteoNeuroGen Inc, and J-H Kim and Y-M Yoon are employed by OsteoNeuroGen. The anti-fibrosis capability of chromones is the subject of a Korean patent, an international PCT and a US patent.

Author contributions

B-S Youn and H-S Kim conceived the idea. I-H Kim coordinated the experiments and helped to write the manuscript. J-H Kim was involved in executing major experiments, JY Lee contributed to real-time imaging, TH Lee gave technical support and conceptual advice and Y-M Yoon took part in chemical screening and the EMT assay. MK Maeng conducted phosphorylation analysis following eupatilin stimulation.

REFERENCES

1. Bonnans, C., Chou, J., and Werb, Z. (2014) Remodelling the extracellular matrix in development and disease. *Nat. Rev. Mol. Cell. Biol.* **15**, 786-801
2. Fallowfield, J. A. (2015) Future mechanistic strategies for tackling fibrosis--an unmet need in liver disease. *Clin. Med. (Lond)* **15 Suppl.**, s83-s87
3. Sgalla, G., Cocconcelli, E., Tonelli, R., and Richeldi, L. (2016) Novel drug targets for idiopathic pulmonary fibrosis. *Expert Rev. Respir. Med.* **26**, 1-13
4. King, C. S., and Nathan, S. D. (2015) Practical considerations in the pharmacologic treatment of idiopathic pulmonary fibrosis. *Curr. Opin. Pulm. Med.* **21**, 479-489
5. Dixon, R. A., and Pasinetti, G. M. (2010) Flavonoids and isoflavonoids: From plant biology to agriculture and neuroscience. *Plant Physiol.* **154**, 453-457
6. Stapleton, A. E., and Walbot, V. (1994) Flavonoids can protect maize DNA from the induction of ultraviolet radiation damage. *Plant Physiol.* **105**, 881-889
7. Leyva-López, N., Gutierrez-Grijalva, E. P., Ambriz-Perez, D. L., and Heredia, J. B. (2016) Flavonoids as cytokine modulators: A possible therapy for inflammation-related diseases. *Int. J. Mol. Sci.* **17**, 921
8. Emami, S., and Ghanbarimasir, Z. (2015) Recent advances of chroman-4-one derivatives: synthetic approaches and bioactivities. *Eur. J. Med. Chem.* **93**, 539-563
9. Gacche, R. N., Meshram, R. J., Shegokar, H. D., Gond, D. S., Kamble, S. S., Dhabadge, V. N., Utage, B. G., Patil, K. K., and More, R. A. (2015) Flavonoids as a scaffold for development of novel anti-angiogenic agents: An experimental and computational enquiry. *Arch. Biochem. Biophys.* **577-578**, 35=48
10. Kim, J. Y., Lee, M. S., Bae, J. M., Park, J., Youn, B. S., and J, O. (2015) Massive elimination of multinucleated osteoclasts by eupatilin is due to dual inhibition of transcription and cytoskeletal rearrangement. *Bone Rep.* **3**, 83-94
11. Huang, S. K., Scruggs, A. M., McEachin, R. C., White, E. S., and Peters-Golden, M. (2014) Lung fibroblasts from patients with idiopathic pulmonary fibrosis exhibit genome-wide differences in DNA methylation compared to fibroblasts from nonfibrotic lung. *PLoS One* **12**, e107055
12. du Bois, R. M. (2010) Strategies for treating idiopathic pulmonary fibrosis. *Nat. Rev. Drug Discov.* **9**, 129-140
13. Morra, L., and Moch, H. (2011) Periostin expression and epithelial-mesenchymal transition in cancer: a review and an update. *Virchows Arch.* **459**, 465-475
14. Kasai, H., Allen, J. T., Mason, R. M., Kamimura, T., and Zhang, Z. (2005) TGF-beta1 induces human alveolar epithelial to mesenchymal cell transition (EMT). *Respir. Res.* **6**, 56
15. Pretheeban, T., Lemos, D. R., Paylor, B., Zhang, R. H., and Rossi, F. M. (2012) Role of stem/progenitor cells in reparative disorders. *Fibrogenesis Tissue Repair* **5**, 20
16. Gabele, E., Brenner, D. A., and Rippe, R. A. (2003) Liver fibrosis: signals leading to the amplification of the fibrogenic hepatic stellate cell. *Front Biosci.* **8**, d69-d77
17. Xie, L., Law, B. K., Chytil, A. M., Brown, K. A., Aakre, M. E., and Moses, H. L. (2004) Activation of the Erk pathway is required for TGF-β1-induced EMT *in vitro*. *Neoplasia* **6**, 603-610
18. Willis, B. C., and Borok, Z. (2007) TGF-beta-induced EMT: mechanisms and implications for fibrotic lung disease. *Am. J. Physiol. Lung Cell. Mol. Physiol.* **293**, L525-L534
19. Wu, Q., Hou, X., Xia, J., Qian, X., Miele, L., Sarkar, F. H., and Wang, Z. (2013) Emerging roles of PDGF-D in EMT progression during tumorigenesis. *Cancer Treat. Rev.* **39**, 640-646
20. Wollin, L., Wex, E., Pautsch, A., Schnapp, G., Hostettler, K. E., Stowasser, S., and Kolb, M. (2015) Mode of action of nintedanib in the treatment of idiopathic pulmonary fibrosis. *Eur. Respir. J.* **45**, 1434-1445

21. Wynn, T. A. (2008) Cellular and molecular mechanisms of fibrosis. *J. Pathol.* **214**, 199-210
22. Ji, H. Y., Lee, H. W., Shim, H. J., Kim, S. H., Kim, W. B., and Lee, H. S. (2004) Metabolism of eupatilin in rats using liquid chromatography/electrospray mass spectrometry. *Biomed. Chromatogr.* **18**, 173-177
23. Strauss, J. F., and Barbieri, R. L. (2014) *Yen & Jaffe's Reproductive Endocrinology : Physiology, Pathophysiology, and Clinical Management*, 7th. Ed. ed., Elsevier Saunders, Philadelphia
24. Verma, N., Kumar, P., Mitra, S., Taneja, S., Dhooria, S., Das, A., Duseja, A., Dhiman, R. K., and Chawla, Y. (2017) Drug idiosyncrasy due to pirfenidone presenting as acute liver failure: Case report and mini-review of the literature. *Hepatol. Commun.* **2**, 142-147
25. Trapnell, C., Roberts, A., Goff, L., Pertea, G., Kim, D., Kelley, D. R., Pimentel, H., Salzberg, S. L., Rinn, J. L., and Pachter, L. (2012) Differential gene and transcript expression analysis of RNA-seq experiments with TopHat and Cufflinks. *Nat. Protoc.* **7**, 562-578
26. Sun, J., Nishiyama, T., Shimizu, K., and Kadota, K. (2013) TCC: an R package for comparing tag count data with robust normalization strategies. *BMC Bioinformatics* **14**, 219
27. Szklarczyk, D., Franceschini, A., Kuhn, M., Simonovic, M., Roth, A., Minguez, P., Doerks, T., Stark, M., Muller, J., Bork, P., Jensen, L. J., and von Mering, C. (2011) The STRING database in 2011: functional interaction networks of proteins, globally integrated and scored. *Nucleic Acids Res.* **39**, D561-568
28. Geerts, A., Eliasson, C., Niki, T., Wielant, A., Vaeyens, F., and Pekny, M. (2001) Formation of normal desmin intermediate filaments in mouse hepatic stellate cells requires vimentin. *Hepatol.* **33**, 177-188

Figure legends

Figure 1. Inhibition of TGFβ-induced fibrogenesis by eupatilin. (A) DHLFs (5×10^6 cells) were seeded in fibroblast growth medium (FBM), grown overnight, and then stimulated with control medium, TGFβ (5 ng/ml), or TGFβ plus eupatilin (50 μM) for 72 hr. Morphological change was monitored by phase-contrast microscopy at 40× magnification. (B) DHLFs were stimulated as described above, and ICC was performed using antibody against mouse α-smooth muscle actin. Nuclei were detected by DAPI staining. (C) Total RNA was isolated from DHLFs stimulated with control medium, TGFβ, or TGFβ plus eupatilin for 48 hr, and then subjected to real-time PCR analysis using primers against *periostin* or *vimentin*. Standard deviations were calculated from the results of three independent PCRs. (D) ONGHEPA1 cells were stimulated with TGFβ (5 ng/ml) or TGFβ plus eupatilin (50 μM) for 24 hr, and morphological changes were monitored under a light microscope. ICC was performed using anti-mouse α-smooth muscle actin. (E) Total RNAs were isolated from ONGHEPA1 cells stimulated with medium, TGFβ, or TGFβ plus eupatilin for 48 hr, and then subjected to real-time PCR analysis using primers against *collagen11α1*. (F) ONGHEPA1 cells were grown and stimulated with medium, eupatilin, pirfenidone, or nintedanib in the presence or absence of TGFβ for 24 hr, and then anti-fibrogenesis was monitored. (G) ONGHEPA1 cells were stimulated as described above, and ICC was performed using antibody against mouse α-smooth muscle actin. Nuclei were detected by DAPI staining.

Figure 2. Administration of eupatilin to bleomycin-treated mice significantly improves lung fibrosis. (A) Vehicle (0.5% CMC + 1% Tween 80), pirfenidone (100 mpk), or various concentrations of eupatilin (10, 50, 100, or 200 mpk) were orally administered into C57BL/6J mice 1 day before administration of bleomycin. Bleomycin was intratracheally injected, and the drugs were administered orally twice per day for 14 days, after which lung tissues and plasma were collected. Histomorphometry was performed. Statistical significance was calculated by Student's *t*-test (*, $p<0.05$; **, $p<0.01$). (B) Levels of hydroxyproline were measured and subjected to Student's *t*-test as described above. ***, $p<0.001$. (C) Whole right lung tissue lysates were subjected to a mouse TGFβ ELISA. (D) Paraffin sections of lung tissues were stained with H&E and Sirius Red, and then observed by phase-contrast microscopy (10× magnification).

Figure 3. Structure–activity relationship of a selected group of chromone derivatives. (A) Chemical structure of the general chromone scaffold, with its carbons denoted in colored fonts. C2, C3, C6, and C7 are critical for anti-fibrogenesis. (B) ONGHEPA1 cells were simultaneously stimulated with control medium, TGFβ, or TGFβ plus eupatilin (50 μM). Anti-fibrogenic effects were observed by phase-contrast light microscopy. (C) Anti-fibrogenic effects of ONGH300 were observed by phase-contrast light microscopy. (D) Anti-fibrogenic effects of ONGI200 (also called apigenin) were observed by phase-contrast light microscopy. (E) A list of 35 CDs, grouped by chemical moieties coupled to the chromone scaffolds or the phenyl ring. Group A including eupatilin, ONGA300 (jaceosidin), and ONGH300 (hispidulin) exerted potent anti-fibrogenic capacity.

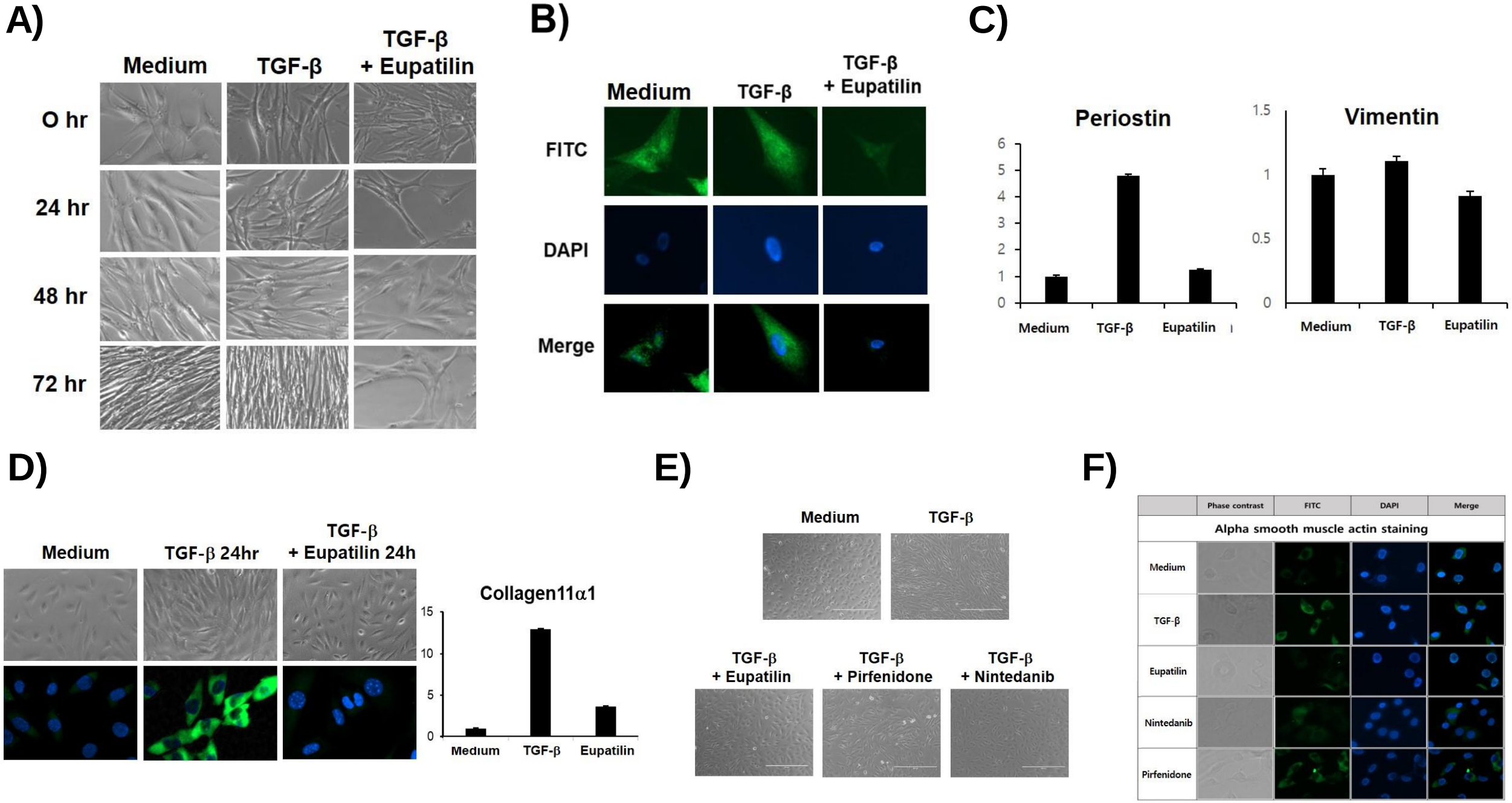
A)
Medium
TGF-β
TGF-β + Eupatilin
O hr
24 hr
48 hr
72 hr
B)
Medium
TGF-β
TGF-β + Eupatilin
FITC
DAPI
Merge
C)
Periostin
Vimentin
Medium
TGF-β
Eupatilin
D)
Medium
TGF-β 24hr
TGF-β + Eupatilin 24h
Collagen11α1
Medium
TGF-β
Eupatilin
E)
Medium
TGF-β
TGF-β + Eupatilin
TGF-β + Pirfenidone
TGF-β + Nintedanib
F)
Phase contrast
FITC
DAPI
Merge
Alpha smooth muscle actin staining
Medium
TGF-β
Eupatilin
Nintedanib
Pirfenidone

Figure 1

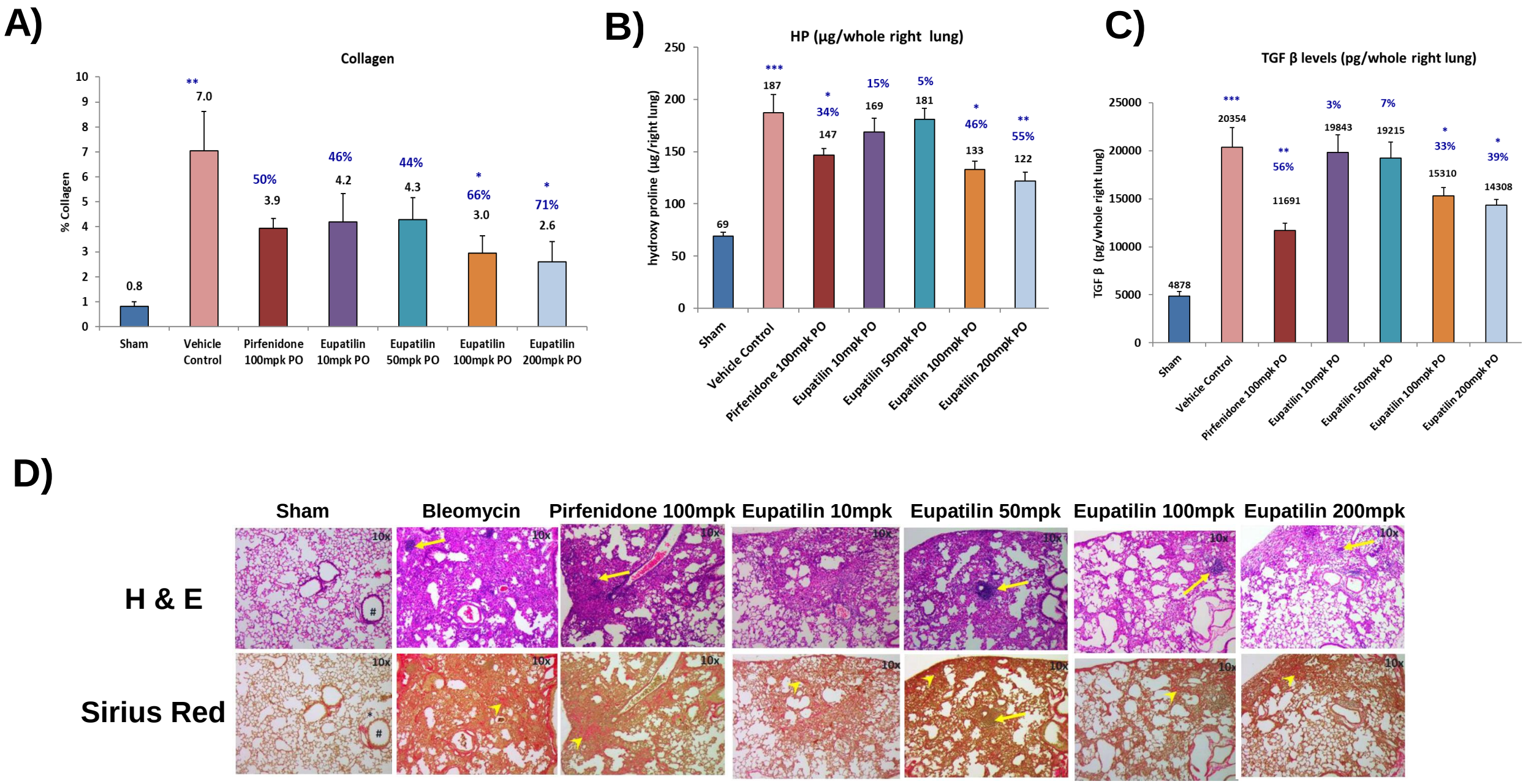
A)
Collagen
% Collagen
0.8
7.0
3.9
4.2
4.3
3.0
2.6
50%
46%
44%
66%
71%
Sham
Vehicle Control
Pirfenidone 100mpk PO
Eupatilin 10mpk PO
Eupatilin 50mpk PO
Eupatilin 100mpk PO
Eupatilin 200mpk PO
B)
HP (µg/whole right lung)
hydroxy proline (µg/right lung)
69
187
147
169
181
133
122
34%
15%
5%
46%
55%
C)
TGF β levels (pg/whole right lung)
TGF β (pg/whole right lung)
4878
20354
11691
19843
19215
15310
14308
56%
3%
7%
33%
39%
D)
Sham
Bleomycin
Pirfenidone 100mpk
Eupatilin 10mpk
Eupatilin 50mpk
Eupatilin 100mpk
Eupatilin 200mpk
H & E
Sirius Red
10x

Figure 2

A)

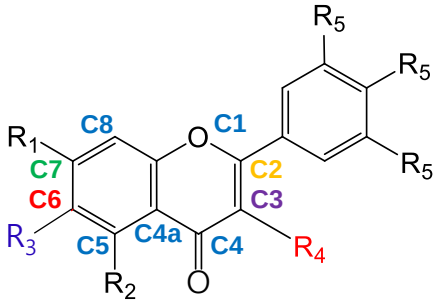

B)

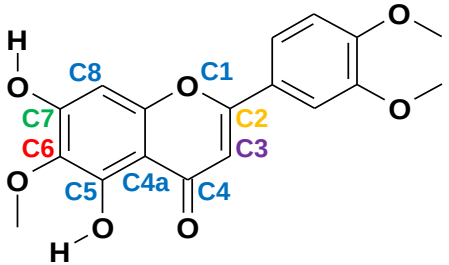

2-(3,4-dimethoxyphenyl)-5,7-dihydroxy-6-methoxy-4H-chromen-4-one **(Eupatilin)**

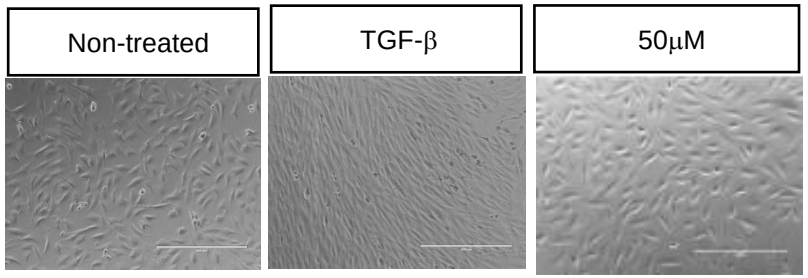

C)

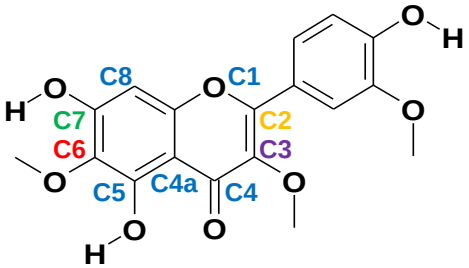

3,6-dimethoxy-4H-chromen-4-one 5,7-dihydroxy-2-(4-hydroxy-3-methoxyphenyl (**ONGH300**)

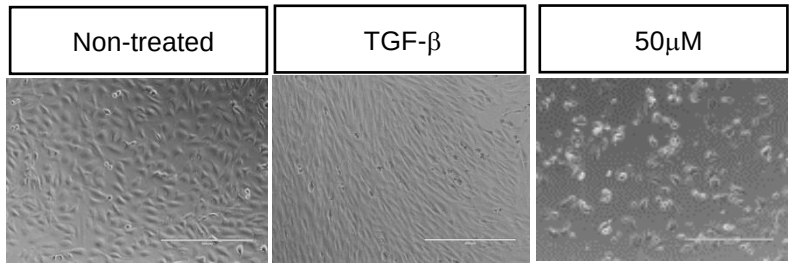

D)

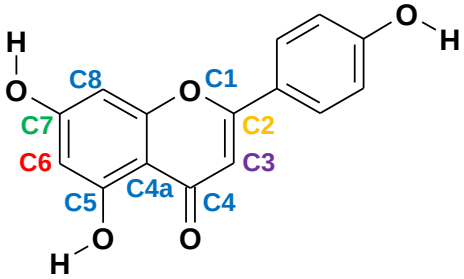

5,7-dihydroxy-2-(4-hydroxyphenyl)-4H-chromen-4-one (**ONGI200**)(**Apigenin**)

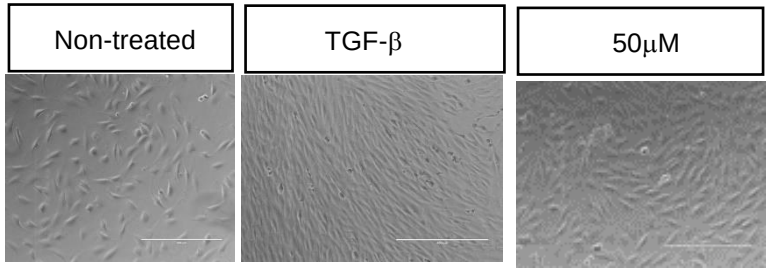

E)

	Compound	R1	R2	R3	R4	R5	R6	R7	Anti-Fibrosis
	Eupatilin	OH	OH	OMe	H	H	OMe	OMe	++++
Group A	ONGE200	OH	OH	OMe	H	H	OH	H	+++
Group A	ONGA300	OH	OH	OMe	H	H	OH	OMe	++
Group A	ONGI300	OH	OH	OMe	H	OH	OH	H	-
Group B	ONGG200	OH	OH	H	H	H	H	H	-
Group B	ONGF300	OH	OH	OMe	OMe	H	H	H	-
Group B	ONGH300	OH	OH	OMe	OMe	H	OH	OMe	-
Group B	ONGB400	OH	OH	OMe	H	H	OMe	H	-
Group B	ONGD400	OH	OH	OMe	OMe	H	OMe	OH	-
Group B	ONGA100	OH	OH	H	OMe	H	H	H	-
Group B	ONGG100	OH	OH	H	OH	H	OH	OH	-
Group B	ONGC300	OMe	OMe	OMe	H	H	OMe	H	-
Group B	ONGG300	OMe	OH	OMe	OMe	H	OH	OH	-
Group C	ONGH100	OMe	OH	OH	H	H	H	H	-
Group C	ONGC200	OMe	OH	OMe	H	H	OH	H	-
Group C	ONGD200	OH	OH	OH	H	H	OMe	H	-
Group C	ONGH200	OMe	OH	OMe	H	OH	OH	H	-
Group C	ONGE400	OMe	OH	OMe	H	H	H	H	-
Group C	ONGG400	OMe	OMe	OMe	H	H	OMe	H	-
Group D	ONGC100	OH	H	H	H	H	OH	H	-
Group D	ONGE100	H	OMe	OH	H	H	H	H	-
Group D	ONGF200	H	H	OMe	H	H	H	H	-
Group D	ONGB300	OH	H	H	H	OH	OH	H	-
Group D	ONGD300	H	H	H	H	H	H	H	-
Group D	ONGA400	OH	H	H	H	H	H	H	-
Group D	ONGF400	H	OH	H	H	H	H	H	-
Group D	ONGE300	OH	OH	H	H	H	OH	OH	-
Group D	ONGH400	H	H	H	H	H	OMe	H	-
Group D	Apigenin	OH	OH	H	H	H	OH	H	-
Group E	ONGB100	OH	OH	H	H	H	H	H	-
Group E	ONGB200	OH	OH	H	OMe	H	OH	H	-
Group E	ONGA200	OMe	OH	H	OMe	OMe	OMe	OH	-
Group E	ONGD100	OH	OH	H	OH	OH	OH	OH	-
Group E	ONGF100	OH	OH	H	OH	H	OH	H	-
Group E	ONGC400	OMe	OMe	H	H	H	OMe	OMe	-

Figure 3